nature neuroscience

Merlin isoform 2 in neurofibromatosis type 2–associated polyneuropathy

Alexander Schulz[1], Stephan L Baader[2,12], Michiko Niwa-Kawakita[3,11,12], Marie Juliane Jung[1], Reinhard Bauer[4], Cynthia Garcia[5], Ansgar Zoch[1], Stephan Schacke[1], Christian Hagel[6], Victor-Felix Mautner[7], C Oliver Hanemann[8], Xin-Peng Dun[8], David B Parkinson[8], Joachim Weis[9], J Michael Schröder[9], David H Gutmann[5], Marco Giovannini[10] & Helen Morrison[1]

The autosomal dominant disorder neurofibromatosis type 2 (NF2) is a hereditary tumor syndrome caused by inactivation of the *NF2* tumor suppressor gene, encoding merlin. Apart from tumors affecting the peripheral and central nervous systems, most NF2 patients develop peripheral neuropathies. This peripheral nerve disease can occur in the absence of nerve-damaging tumors, suggesting an etiology that is independent of gross tumor burden. We discovered that merlin isoform 2 (merlin-iso2) has a specific function in maintaining axonal integrity and propose that reduced axonal *NF2* gene dosage leads to NF2-associated polyneuropathy. We identified a merlin-iso2–dependent complex that promotes activation of the GTPase RhoA, enabling downstream Rho-associated kinase to promote neurofilament heavy chain phosphorylation. Merlin-iso2–deficient mice exhibited impaired locomotor capacities, delayed sensory reactions and electrophysiological signs of axonal neuropathy. Sciatic nerves from these mice and sural nerve biopsies from NF2 patients revealed reduced phosphorylation of the neurofilament H subunit, decreased interfilament spacings and irregularly shaped axons.

Neurons of both the peripheral nervous system (PNS) and central nervous system (CNS) are highly polarized complex cellular units. During development, several morphological steps are required for normal functioning and plasticity of the developing nervous system. New neurons migrate to their appropriate locations, extend axons and dendrites into the correct target regions, and form synapses with their partners. These distinct morphological processes depend on the spatiotemporal control of intrinsic neuronal signaling networks in which the Rho family of small GTPases are important regulatory components[1]. The signaling mechanisms that establish these highly plastic neuronal processes are well characterized, but the manner in which these neurons achieve and maintain more stable structures, such as axon radial growth over far-reaching distances, throughout life is less well understood.

Neurofilaments are at least one component known to be required to promote and maintain radial growth also known as axonal caliber[2]. Neurofilaments are neuron-specific intermediate filaments composed of NF-H (200 kDa), NF-M (150 kDa) and NF-L (68 kDa) subunits. To date, transcriptional upregulation[3] and/or extensive side-arm phosphorylation of the NF-M or NF-H subunits[4] are thought to determine structural integrity in axons[2], whereas the upstream signaling mechanisms that control and modify neurofilaments are not well characterized. *Nefl* (which encodes NF-L) gene disruption in mice results in loss of neurofilaments and subsequent failure of axons to grow radially[5]. Neurofilament abnormalities in humans have been documented in a number of neurological diseases, including several inherited neuropathies[2]. Inherited genetic mutations related to neurofilaments induce axonal alterations that result in nerve damage, leading to typical neuropathic symptoms, such as loss of sensation, pain or muscular weakness[6].

NF2 is a hereditary tumor syndrome caused by inactivation of the *NF2* tumor suppressor gene encoding merlin. Apart from gliogenic tumors in the PNS and CNS, most NF2 patients develop peripheral neuropathies[7,8]. NF2-related neuropathy mostly appears in a symmetric and distal manner and occurs in the absence of compressive spinal or peripheral tumors[8], indicating a systemic, rather than focal, etiology. This suggests the involvement of factors other than gross tumor burden.

We identified a function for merlin in neurons of the developing CNS[9]. At least two alternatively spliced merlin variants are expressed: merlin isoform 1 (merlin-iso1), which lacks exon 16, and merlin-iso2, which contains exon 16 and encodes a C-terminally truncated protein. Merlin-iso1 has been established as a tumor suppressor, but little is known about merlin-iso2's function. We found that both merlin

[1]Leibniz Institute for Age Research, Fritz Lipmann Institute, Jena, Germany. [2]Institute of Anatomy, Anatomy and Cell Biology, University of Bonn, Bonn, Germany. [3]Inserm U674, Université Paris, Paris, France. [4]Institute of Molecular Cell Biology and Center for Sepsis Control and Care, Jena University Hospital, Friedrich Schiller University, Jena, Germany. [5]Department of Neurology, Washington University School of Medicine, St. Louis, Missouri, USA. [6]Department of Neuropathology, University Medical Center Hamburg-Eppendorf, Hamburg, Germany. [7]Department of Neurology, University Medical Center Hamburg-Eppendorf, Hamburg, Germany. [8]Plymouth University Peninsula Schools of Medicine and Dentistry, Plymouth, UK. [9]Institute of Neuropathology, RWTH Aachen, University Hospital Aachen, Aachen, Germany. [10]House Ear Institute, Center for Neural Tumor Research, Los Angeles, California, USA. [11]Present address: Inserm U944, CNRS U7212, Université Paris, Institut Universitaire d'Hématologie, Paris, France. [12]These authors contributed equally to this work. Correspondence should be addressed to H.M. (helen@fli-leibniz.de).

Received 10 September 2012; accepted 30 January 2013; published online 3 March 2013; doi:10.1038/nn.3348

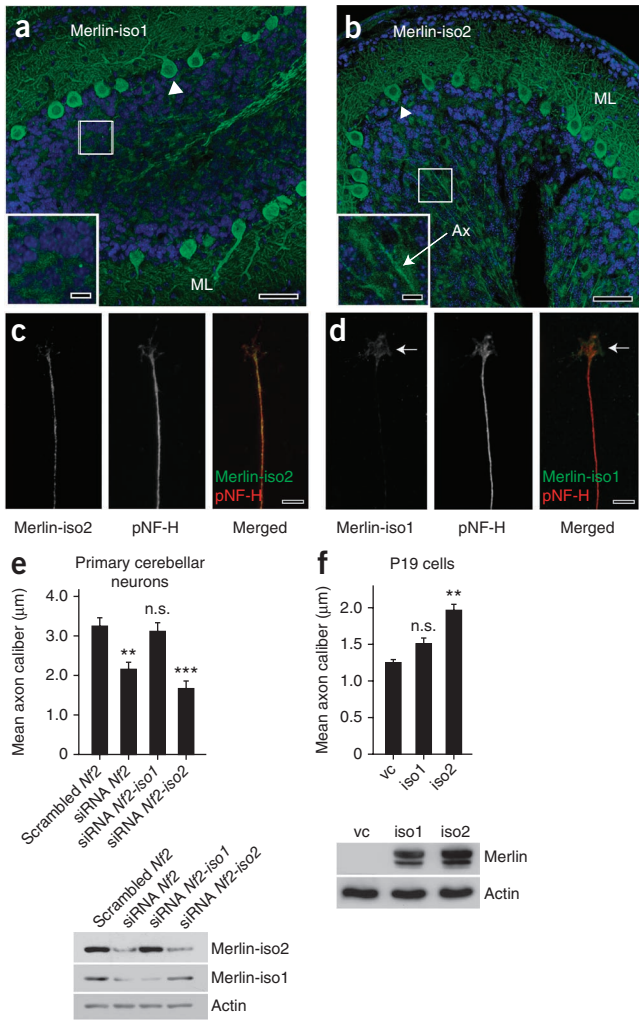

Figure 1 Merlin-iso2 expressed in axons, mediates neurofilament phosphorylation and axonal radial growth. (**a**,**b**) Merlin-iso1 (**a**) and merlin-iso2 (**b**) immunolabeling in the cerebellar cortex at postnatal day 15. Merlin-iso2 was expressed in Purkinje cell axons (Ax arrow). Arrowheads indicate Purkinje cell somata. Molecular layer (ML) is mainly composed of Purkinje cell dendrites. Scale bars represent 75 μm and 15 μm (magnified images). White boxes indicate areas shown at higher magnification. We quantified merlin-iso2 expression in Purkinje cell axons during postnatal development (P3–15) and in adults (P3, 0%; P5, 0%; P9, 5.15%; P15, 45.53%; adult, 96.92%; $n = 50$ axons from 2 mice for each investigated age). (**c**,**d**) Merlin isoform–specific immunolabeling (green) in primary DRG neurons. Co-staining with phosphorylated neurofilaments (pNF-H, red) indicates expression in axons. Merlin-iso1 was present in axonal growth cones (arrows) and merlin-iso2 was detected along the whole axon. Scale bars represent 20 μm. (**e**,**f**) Quantification of axon diameters following specific knockdown (duplexes) in primary cerebellar neurons ($^{**}P < 0.01$, $t = 4.119$, degrees of freedom (df) = 20; $^{***}P < 0.001$, $t = 5.809$, df = 20; $n = 393$ cells from 3 mice; mean + s.e.m.; n.s., not significant, $P = 0.16$). Scrambled control (scrambled *Nf2*), both isoforms (siRNA *Nf2*), merlin-iso1 (siRNA *Nf2-iso1*), merlin-iso2 (siRNA *Nf2-iso2*) or following overexpression in differentiated P19 cells are shown in **e**. Empty vector control (vc), merlin-iso1 (iso1), merlin-iso2 (iso2) are shown in **f** ($^{**}P < 0.01$, $t = -8.201$, df = 19; $n = 460$ cells; mean + s.e.m.; n.s., not significant, $P = 0.07$). Immunoblots for actin (loading control), merlin-iso1 and merlin-iso2 or merlin were used to confirm knockdown and overexpression. Merlin overexpression migrated as a doublet; the upper band representing phosphorylated merlin and the lower band represented dephosphorylated merlin. For full-length blots and quantitations, see **Supplementary Figure 3**.

isoforms were able to restrict dendritic morphogenesis through inhibition of the small GTPase Rac1 (ref. 9). Our finding suggest that merlin, a known tumor suppressor, is involved in controlling highly plastic neuronal processes such as dendrites in the developing brain. We hypothesize that merlin may also function in the development and maintenance of more stable structures such as axons, and suggest that the specific loss or reduction of merlin in neurons may contribute to NF2-related polyneuropathy.

RESULTS

Merlin-iso2 mediates neurofilament phosphorylation

Using isoform-specific antibodies, we detected both merlin isoforms in cerebellar Purkinje cell somata (**Fig. 1a**,**b**) and dendrites in the molecular layer. Only isoform 2 was localized to axonal processes running from Purkinje cells toward the white cerebellar matter (**Fig. 1a**,**b** and **Supplementary Fig. 1**).

Merlin-iso2–positive signals in Purkinje cells began to appear between postnatal days 9 and 15 (P9 and P15) in Purkinje cell axons (**Fig. 1** and Online Methods), coinciding with a period of Purkinje cell axonal maturation characterized by extensive neurofilament phosphorylation and diameter adjustment[10]. In addition, we detected predominant merlin-iso2 expression in cells belonging to the PNS, including sciatic nerve axons (**Supplementary Fig. 2**) and axons of primary dorsal root ganglion (DRG) cells (**Fig. 1c**,**d**).

We used primary neuronal monocultures independent of the associated influence of glial cells and the murine embryonic carcinoma P19 cell line, which are known to differentiate into neuronal cells[11], to investigate whether merlin-iso2 affects axon–intrinsic morphogenesis. Specific knockdown of merlin-iso2 or of both isoforms in isolated primary cerebellar neurons decreased axonal diameter, whereas merlin-iso1–specific knockdown had no detectable influence (**Fig. 1e** and **Supplementary Fig. 3a**). Concordantly, overexpression of merlin-iso2 elicited a substantial increase in axonal diameter compared with overexpression of merlin-iso1 (**Fig. 1f**). The decrease in axonal diameter resulting from merlin-iso2 protein reduction could be rescued by the expression of human merlin-iso2 in mouse P19 cells (**Fig. 2**).

We investigated whether the merlin-iso2 effect on axonal caliber is mediated through neurofilament regulation. Although the total amount of neurofilaments remained unaffected (data not shown), the phosphorylation status of NF-H in primary cerebellar neurons was decreased by merlin-iso2 knockdown, but merlin-iso1 knockdown (**Fig. 2a**). Accordingly, merlin-iso2 overexpression led to a robust neurofilament phosphorylation in P19 cells, whereas merlin-iso1 overexpression had only minor effects (**Fig. 2b**). Taken together, these findings establish a specific intrinsic neuronal role of merlin-iso2 in the regulation of neurofilament phosphorylation that leads to radial axonal growth.

Axonal merlin-iso2 involves RhoA signaling

Neurofilaments are phosphorylated by several serine/threonine kinases[2]. Because merlin lacks any endogenous kinase activity, we screened for serine/threonine kinases that were involved in merlin and/or neurofilament signaling (**Supplementary Table 1**). We monitored whether the knockdown of each tested kinase could prevent or decrease neurofilament phosphorylation following merlin-iso2 overexpression *in vitro*. One of the kinases that we identified, Rho-associated kinase (ROCK), has been reported to directly phosphorylate neurofilaments *in vitro*[12]. Overexpression of merlin-iso2

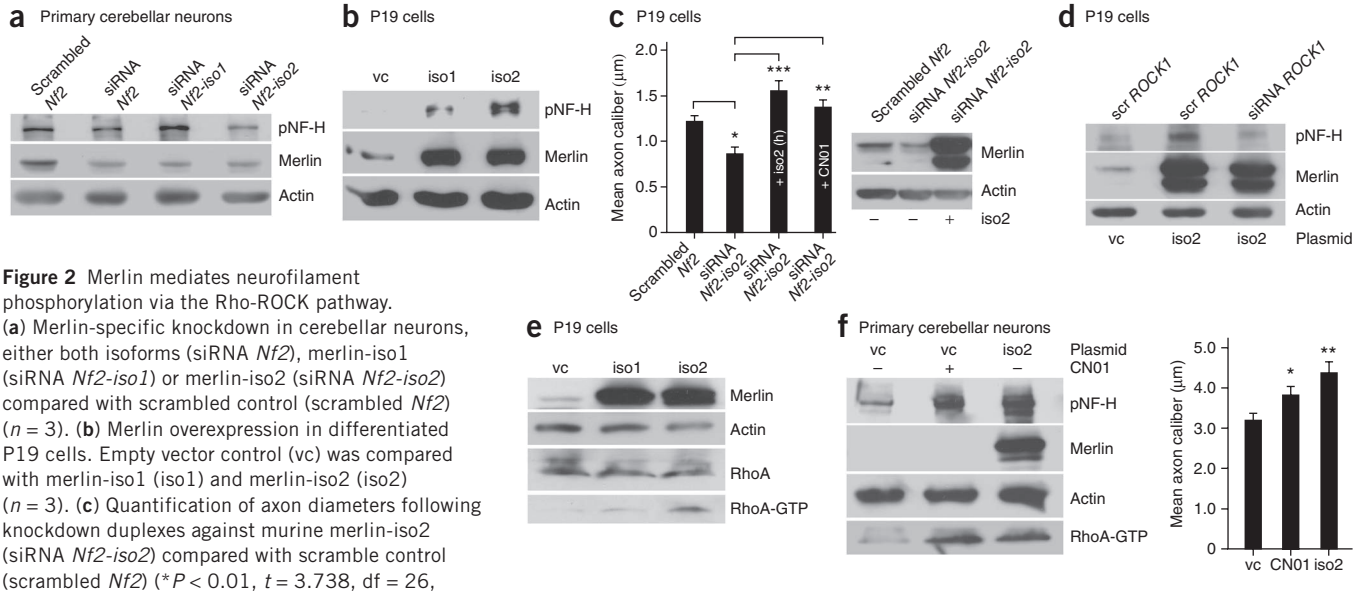

Figure 2 Merlin mediates neurofilament phosphorylation via the Rho-ROCK pathway. (**a**) Merlin-specific knockdown in cerebellar neurons, either both isoforms (siRNA *Nf2*), merlin-iso1 (siRNA *Nf2-iso1*) or merlin-iso2 (siRNA *Nf2-iso2*) compared with scrambled control (scrambled *Nf2*) ($n = 3$). (**b**) Merlin overexpression in differentiated P19 cells. Empty vector control (vc) was compared with merlin-iso1 (iso1) and merlin-iso2 (iso2) ($n = 3$). (**c**) Quantification of axon diameters following knockdown duplexes against murine merlin-iso2 (siRNA *Nf2-iso2*) compared with scramble control (scrambled *Nf2*) (*$P < 0.01$, $t = 3.738$, df = 26, $n = 102$ cells, mean + s.e.m.), co-transfection with human merlin-iso2 (+iso2) or treatment with Rho activator (+CN01) (**$P < 0.01$, $t = –4.782$, df = 27; ***$P < 0.001$, $t = –5.596$, df = 24; $n = 112$ cells, mean + s.e.m.). Right, immunoblot for merlin and actin confirmed effective knockdown and transfection levels ($n = 3$). (**d**) ROCK knockdown prevented merlin-iso2–induced neurofilament phosphorylation. P19 cells were treated with scrambled control duplexes (scr) and empty vector control, scr and merlin-iso2 overexpression (iso2), siRNA ROCK and merlin-iso2 overexpression (*ROCK1*/iso2) ($n = 3$). (**e**) P19 cells were measured for RhoA-GTP level after merlin-iso2 (iso2) and merlin-iso1 (iso1) overexpression compared with empty vector control (vc) ($n = 3$). (**f**) RhoA-GTP level was measured in cerebellar neurons after treatment with Rho activator (CN01) or overexpression with merlin-iso2 (iso2) compared with vector control (vc) ($n = 3$). Right, radial axonal growth (*$P < 0.05$, $t = –2.381$, df = 23, $n = 98$ cells from 3 mice; **$P < 0.01$, $t = –3.804$, df = 22, $n = 116$ cells from 3 mice; mean + s.e.m.). For full-length blots and quantitations, see **Supplementary Figures 3** and **4**.

and simultaneous silencing of ROCK using siRNA prevented merlin-iso2–specific NF-H phosphorylation (**Fig. 2d**), suggesting that merlin-iso2 acts upstream of ROCK.

To elucidate how merlin-iso2 regulates ROCK, we examined the activity of the GTPase RhoA, an upstream regulator of ROCK. Merlin-iso2, but not merlin-iso1, overexpression activated RhoA in P19 cells (**Fig. 2e**). In primary neurons, merlin-iso2 overexpression was mimicked by the application of a Rho activator (CN01), as indicated by increased RhoA activity, NF-H phosphorylation and an increase in axonal caliber (**Fig. 2f**). Furthermore, application of the same Rho activator alone could rescue the axonal caliber decrease following merlin-iso2 repression in P19 cells (**Fig. 2c**).

In addition to the CNS, we found that merlin-iso2 function is important in PNS neurons. We isolated glia-free primary DRG cells whose axons (known as afferents) relay sensory information into the CNS. A merlin-iso2–specific knockdown in these cells resulted in a decrease in neurofilament phosphorylation (**Fig. 3a**). We also examined the effect of merlin loss using genetically engineered mice bearing complete isoform-specific knockouts of merlin, designated *Nf2-iso1*$^{-/-}$ and *Nf2-iso2*$^{-/-}$. We confirmed merlin isoform–specific knockout at the protein level in forebrain and hindbrain lysates (**Supplementary Fig. 4c**). As expected, neurofilament phosphorylation was predominantly reduced in *Nf2-iso2*$^{-/-}$ brains (**Supplementary Fig. 4c**). Similar to CNS nerve cells, *in vitro* DRG neurons isolated from *Nf2-iso2*$^{-/-}$ mice had smaller axonal diameters than wild-type control and *Nf2-iso1*$^{-/-}$ mice (**Fig. 3b**). Moreover, *Nf2-iso2*$^{-/-}$ DRG neurons could be rescued by expression of merlin-iso2, with a substantial RhoA activation accompanied by neurofilament phosphorylation and subsequent radial axonal growth (**Fig. 3c** and **Supplementary Fig. 4d**). Transfection of a constitutively active form of RhoA (RhoA 63L) into DRG cells[13] resulted in an increase in neurofilament phosphorylation and axonal caliber growth (**Fig. 3d**).

These data indicate that RhoA activity contributes to axonal diameter adjustment in both the CNS and PNS. Our data imply that part of merlin-iso2's mechanism of action involves activation of RhoA, enabling downstream ROCK to promote neurofilament phosphorylation.

Merlin assembles a multi–protein complex

Guanine nucleotide exchange factors (GEFs), GTPase-activating proteins (GAPs) and GDP dissociation inhibitors (GDIs) are considered to be the primary determinants in neuronal Rho regulation. Our data indicate that merlin is involved in controlling Rho activity, specifically axonal caliber growth in neurons *in vitro*. We therefore explored how merlin-iso2 might operate in the axon to promote Rho signaling.

Because merlin has been suggested to interact with the guanine nucleotide dissociation inhibitor RhoGDI[14], as well as with p190RhoGAP (unpublished observations), in other cell types, we hypothesized the existence of a neurofilament-associated multi-protein complex in which merlin-iso2 regulates RhoA activity in neurons. Both RhoGDI and p190RhoGAP were expressed in DRG cell axons (**Supplementary Fig. 4f** and **5a**). The reduction of either RhoGDI or p190RhoGAP in neuronal cells led to an increase in Rho activity, neurofilament phosphorylation and radial axonal growth (**Fig. 3e** and **Supplementary Fig. 5c,d**), establishing the importance of these regulatory components *per se* in axonal Rho activity control.

In wild-type mouse sciatic nerves, the levels of the two major merlin isoforms, RhoA and RhoGDI remained unchanged during development (**Supplementary Fig. 5e–g**). The level of p190RhoGAP appeared to be higher at birth (P0) and was reduced around P20, coinciding with axonal maturation characterized by extensive neurofilament phosphorylation (**Supplementary Fig. 5g**).

Notably, the sciatic nerves of adult *Nf2-iso2*$^{-/-}$ mice (P60) showed reduced levels of active RhoA (RhoA-GTP) and reduced

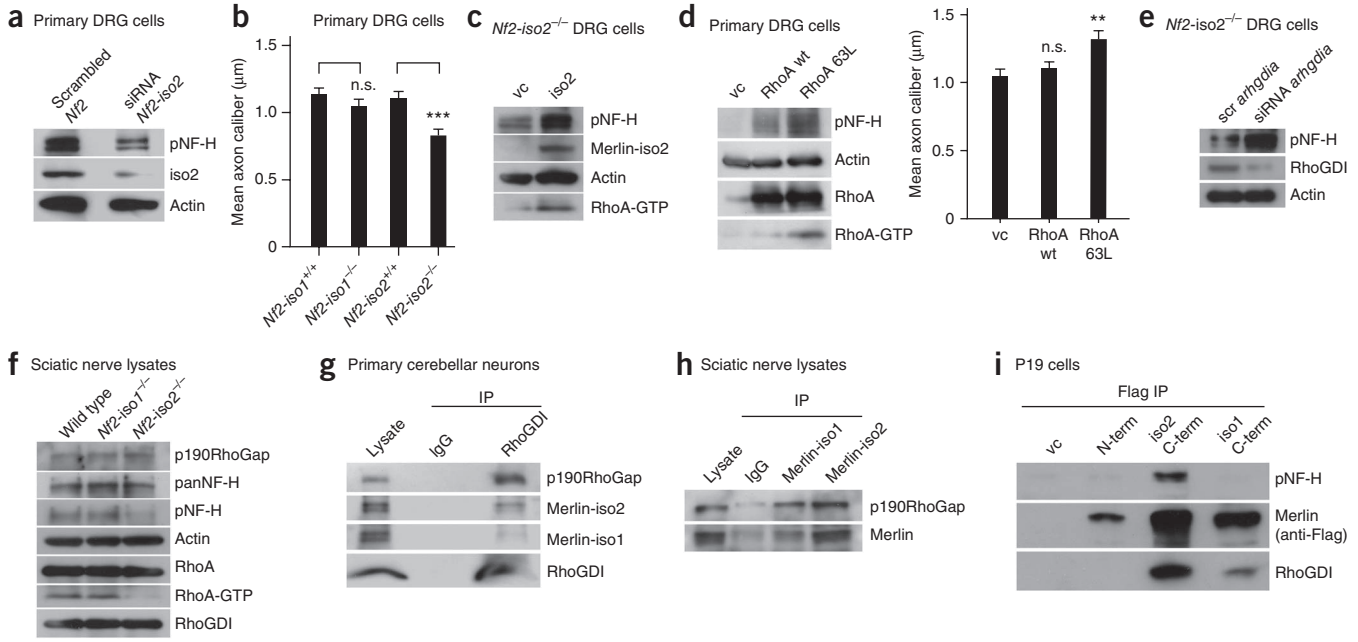

Figure 3 Merlin assembles a multi-protein complex relevant for Rho activation. (**a**) Merlin-iso2–specific knockdown (siRNA *Nf2-iso2*) in primary DRG neurons compared with scrambled duplex control (scr *Nf2*) ($n = 3$). (**b**) DRG neurons were isolated from isoform-specific knockout mice and axonal calibers were measured. *Nf2-iso2*$^{-/-}$ mice compared with *Nf2-iso1*$^{-/-}$ and wild-type controls (*Nf2-iso2*$^{+/+}$ and *Nf2-iso1*$^{+/+}$) ($***P < 0.001$, $t = -2.687$, df = 28, $n = 365$ cells from 3 mice, mean + s.e.m.; n.s., not significant, $P = 0.11$). (**c**) DRG neurons prepared from *Nf2-iso2*$^{-/-}$ transfected with merlin-iso2 (iso2) compared with empty vector control (vc) ($n = 3$). (**d**) Wild-type DRG cells transfected with constitutively active RhoA mutant (RhoA 63L) compared with wild-type RhoA (RhoA wt) and empty vector control (vc) ($n = 3$). Right, radial axon growth *in vitro* ($**P < 0.01$, $t = -3.045$, df = 65, $n = 361$ cells from 3 mice, mean + s.e.m.; n.s., not significant). (**e**) Knockdown of RhoGDI (siRNA *arhgdia*) compared with scrambled control duplexes (scr *arhgdia*) in *Nf2-iso2*$^{-/-}$ DRGs ($n = 3$). (**f**) Sciatic nerve lysates from *Nf2-iso2*$^{-/-}$ mice compared with *Nf2-iso1*$^{-/-}$ mice and wild-type mice ($n = 4$). (**g**) Immunoprecipitation (IP) of endogenous RhoGDI from primary neurons compared with IgG control ($n = 3$). (**h**) Immunoprecipitation from sciatic nerve lysates using merlin-specific antibodies (merlin-iso1 and merlin-iso2) compared with IgG control ($n = 3$). (**i**) Flag-tagged merlin N-terminal fragments (N-term), C-terminal (iso2 C-term and iso1 C-term) and empty vector control (vc) were transfected into P19 cells and immunoprecipitated with antibody to Flag ($n = 4$). For full-length blots and quantitations, see **Supplementary Figures 4–6**.

phosphorylated neurofilaments (**Fig. 3f**). However, the total protein amounts of p190RhoGAP, RhoA and RhoGDI remained unchanged, indicating that the reduction of merlin-iso2 has no effect on the expression and/or stability of these components in adult mice.

Using immunoprecipitation, we confirmed the existence of a multi-protein complex and examined its composition. Antibodies to RhoGDI co-precipitated both merlin isoforms, as well as p190RhoGAP from primary granule cell lysates (**Fig. 3g**). Antibodies to merlin–iso2 and merlin–iso1 both co-precipitated p190RhoGAP from sciatic nerve lysates (**Fig. 3h**). The fact that merlin-iso2 differs from merlin-iso1 in the C terminus, a precise function distinct from the C-terminal merlin-iso1 is suggested. We tested whether a C-terminal fragment of merlin-iso2 was sufficient to associate with neurofilaments. Indeed, only the C-terminal merlin-iso2 co-immunoprecipitated with phosphorylated neurofilaments (**Fig. 3i** and **Supplementary Fig. 6**), indicating that, although both full-length isoforms can form a complex with RhoGDI and p190RhoGAP, merlin-iso2 likely acts locally in axons.

We examined the interaction between merlin and RhoGDI *in vitro* (**Supplementary Fig. 7**). No interaction was detected *in vitro* using purified merlin full-length proteins (**Supplementary Fig. 7a**,**b**). An interaction could only be shown with the FERM domain of merlin (N terminus, shared by the two isoforms) using both purified GST- and His-tagged RhoGDI. We next tested whether merlin acts as a RhoGDI displacement factor (that is, releases inactive RhoA-GDP from RhoGDI to result in RhoA activation). In an *in vitro* Rho activity assay[15], addition of a Rho GEF induced a rapid nucleotide exchange. Addition of RhoGDI sufficiently inhibited this exchange by maintaining RhoA in its inactive form. Inclusion of N-terminal merlin (FERM domain) did not affect the intrinsic RhoA GTP loading or the activity of Rho GEF toward RhoA (**Supplementary Fig. 7c**) and was unable to induce release of RhoGDI from RhoA (**Supplementary Fig. 7c**). Taken together, at least in this *in vitro* assay, we could not detect merlin-dependent inhibition of RhoGDI. Other partners might be required for a complete merlin-dependent RhoGDI displacement from RhoA *in vivo*. In addition, *in vivo* full-length merlin has distinct molecular conformations[16] that may be required to bind and control RhoGDI activity coordinating RhoA signal activation.

Analysis of merlin isoform–specific knockout mice

The availability of isoform-specific *Nf2* knockout mice enabled us to test merlin-iso2–specific functions in an intact nervous system and to determine whether merlin-iso2 loss contributes to an axonal pathogenesis of NF2-associated polyneuropathy. On the basis of our *in vitro* data, we expected these mice to display axonal structure alterations resulting from irregular neurofilament phosphorylation. Because aberrant axonal signals can induce secondary Schwann cell changes in older mice[17], we studied young mice (2 months old), which allowed us to concentrate on specific axonal changes. Our initial studies revealed that both mouse lines appeared to be devoid of NF2-typical tumors, suggesting a compensatory potential for the two major merlin isoforms (unpublished data).

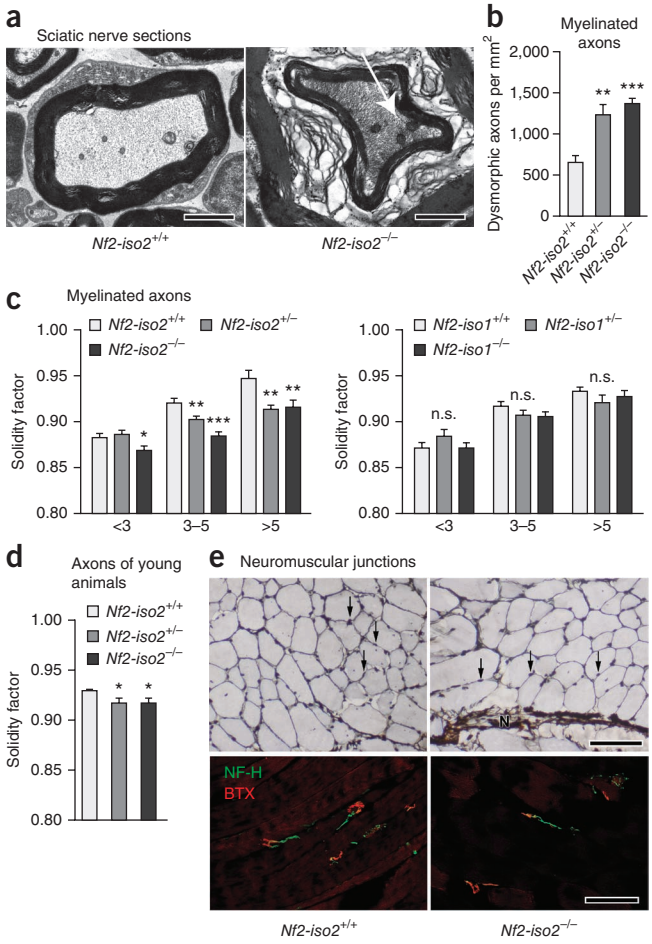

Figure 4 Axon structure abnormalities in *Nf2-iso2*$^{-/-}$ mice. (**a**) Electron micrographs of sciatic nerve axons from *Nf2-iso2*$^{-/-}$ mice compared with *Nf2-iso2*$^{+/+}$ mice. Arrow indicates densely packed neurofilaments and mitochondria. Scale bars represent 1 µm. (**b**) More dysmorphic sciatic nerve axons were found in *Nf2-iso2*$^{+/-}$ and *Nf2-iso2*$^{-/-}$ than in *Nf2-iso2*$^{+/+}$ mice (**$P < 0.01$, $t = -3.401$, df = 29; ***$P < 0.001$, $t = -5.578$, df = 34; $n = 542$ axons from 3 mice, mean + s.e.m.). (**c**) The mean solidity factor was decreased in myelinated axons in sciatic nerve cross sections from *Nf2-iso2*$^{+/-}$ and *Nf2-iso2*$^{-/-}$ mice compared with *Nf2-iso2*$^{+/+}$ mice, whereas loss of merlin-iso1 (*Nf2-iso1*$^{-/-}$, *Nf2-iso1*$^{+/-}$ and *Nf2-iso1*$^{+/+}$ mice) had no significant effect (*$P < 0.05$, $t = -5.196$, df = 165; **$P < 0.01$, $t = -7.135$, df = 183; ***$P < 0.001$, $t = -5.871$, df = 169; n.s., not significant; $n = 1,488$ axons from 3 mice, mean + s.e.m.). Axons were categorized according to their diameter (*x* axis represents axon calibers in µm). (**d**) Sciatic nerve axons of young P7 *Nf2-iso2*$^{+/-}$ and *Nf2-iso2*$^{-/-}$ mice showed comparable solidity factors (*$P < 0.05$, $t = -5.677$, df = 1,039, $n = 1,512$ axons from 3 mice, mean + s.e.m.). (**e**) Gastrocnemius muscle fibers of *Nf2-iso2*$^{+/+}$ and *Nf2-iso2*$^{-/-}$ mice were stained with silver impregnation (top) and immunohistochemically for acetylcholine receptor and myelinated nerve fibers (bottom). Muscle fibers are equal in size, without signs of dying muscle cells or accumulation of fat cells or connective tissue. Muscle fibers appear straight and not wrinkled and the cell bodies (arrows) are arranged along the border of the muscle fiber, not centrally. We detected equal amounts of myelinated nerve fibers by NF-H staining and normal amounts and sizes of endplates by bungarotoxin (BTX) staining ($n = 2$ mice per genotype). Scale bars represent 100 µm.

Sciatic nerve axons of *Nf2-iso2*$^{-/-}$ mice exhibited morphological abnormalities, such as misshaped and dysmorphic axons and accumulations of densely packed neurofilaments and mitochondria (**Fig. 4a**,**b**). Axonal shrinkage resulting from an irregular bending of the axonal surface led to a strong reduction in the solidity factor in both heterozygous (*Nf2-iso2*$^{+/-}$) and homozygous (*Nf2-iso2*$^{-/-}$) mice (**Fig. 4c**). Loss of merlin-iso1 had no effect on the roundness of axons. Even young merlin-iso2–deficient mice (P7) displayed a significant reduction in the solidity factor ($P < 0.05$; **Fig. 4d**), indicating that the observed phenotype originates in the early period of axonal structure maintenance. This abnormal phenotype, including axonal atrophy with shrunken and collapsed axons of peripheral nerves, resembles that described in mice with a neurofilament mutation[18]. Although we detected a high number of shrunken axons in *Nf2-iso2*$^{-/-}$ mice, the total number of axons and the overall axon caliber in sciatic nerve sections appeared to be unaffected (**Supplementary Fig. 8a**). Immunohistochemical analysis of longitudinal sciatic nerve sections from *Nf2-iso2*$^{-/-}$ mice, including *Nf2-iso2*$^{-/-}$ DRG cells cultured for 14 d (data not shown), revealed no obvious signs of degeneration,

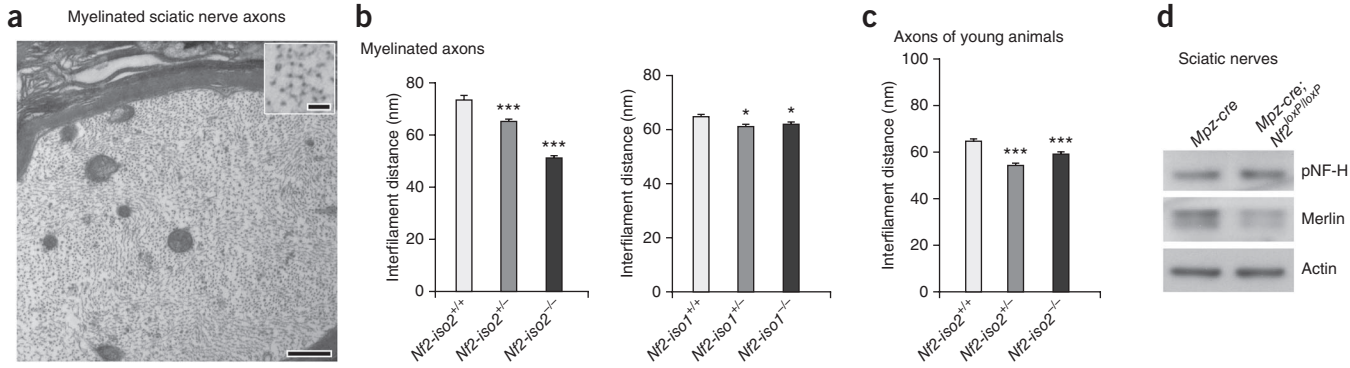

Figure 5 Reduced interfilament distances in *Nf2-iso2*$^{-/-}$ mice. (**a**) Representative electron micrograph of a myelinated sciatic nerve axon. Upper right, 20,000× magnification. Scale bars represent 500 nm and 100 nm (inset). Single neurofilament molecules can be identified as black dots in the axoplasm. (**b**) Distances between single neurofilaments were quantified in sciatic nerve axons of adult *Nf2-iso2*$^{+/-}$ and *Nf2-iso2*$^{-/-}$ mice compared with *Nf2-iso2*$^{+/+}$ mice, and adult *Nf2-iso1*$^{+/-}$ and *Nf2-iso1*$^{-/-}$ mice compared with *Nf2-iso1*$^{+/+}$ mice (*$P < 0.05$, $t = -4.396$, df = 2,968; ***$P < 0.001$, $t = -6.346$, df = 3,021; $n = 3,298$ distances from 3 mice, mean + s.e.m.). (**c**) Young *Nf2-iso2*$^{+/-}$ and *Nf2-iso2*$^{-/-}$ mice compared with *Nf2-iso2*$^{+/+}$ mice (***$P < 0.001$, $t = -6.117$, df = 1,066, $n = 1,454$ distances from 3 mice, mean + s.e.m.). (**d**) Sciatic nerve lysates from *Mpz-cre; Nf2*$^{loxP/loxP}$ mice showed slightly elevated levels of neurofilament phosphorylation compared with control littermates (*Mpz-cre*) ($n = 4$). For full-length blots and quantitations, see **Supplementary Figure 8**.

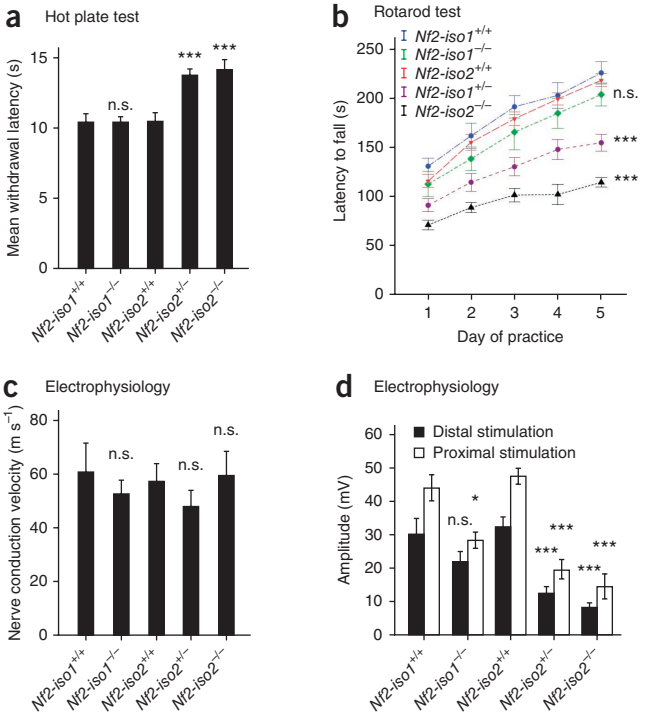

Figure 6 Behavioral abnormalities in *Nf2-iso2*$^{-/-}$ mice. (**a**) Hot plate test measuring response to thermal stimuli revealed greater withdrawal latencies for *Nf2-iso2*$^{+/-}$ and *Nf2-iso2*$^{-/-}$ mice than for *Nf2-iso2*$^{+/+}$ mice (***$P < 0.001$, $t = -4.557$, df = 39; n.s., not significant, $t = 0.007$, df = 15; $n = 8$ mice per group, mean + s.e.m.). (**b**) Rotarod performance of mice trained for 5 consecutive days. *Nf2-iso2*$^{+/-}$ and *Nf2-iso2*$^{-/-}$ mice showed weakened performances compared with *Nf2-iso2*$^{+/+}$, *Nf2-iso1*$^{+/+}$ and *Nf2-iso1*$^{-/-}$ mice (***$P < 0.001$, $t = 6.417$, df = 32; n.s., not significant; $n = 8$ mice per group, mean + s.e.m.). (**c**) Nerve conduction velocities ($n = 6$ mice per group; n.s., not significant) in *Nf2-iso2*$^{+/-}$, *Nf2-iso2*$^{-/-}$ and *Nf2-iso1*$^{-/-}$ mice compared with *Nf2-iso2*$^{+/+}$ and *Nf2-iso1*$^{+/+}$ mice (mean + s.e.m.). (**d**) Compound muscle action potential amplitudes recorded after proximal and distal sciatic nerve stimulation. Amplitudes in both *Nf2-iso2*$^{+/-}$ and *Nf2-iso2*$^{-/-}$ mice were markedly reduced, suggesting axonal-type neuropathy, compared with *Nf2-iso2*$^{-/-}$, *Nf2-iso2*$^{+/+}$ and *Nf2-iso1*$^{+/+}$ mice (*$P < 0.05$, $t = 6.912$, df = 12, $t = 7.280$, df = 10; ***$P < 0.001$; n.s., not significant, $t = 3.377$, df = 10; $n = 6$ per group, mean + s.e.m.).

such as spheroid formations or amyloid precursor protein (APP) accumulations, along axons (**Supplementary Fig. 8b**). As no classical signs of axonal degeneration were detected, we propose that the number of normal functional axons was decreased. However, because axonal integrity is thought to be essential for myelin maintenance, it is possible that an active neurodegeneration may occur in older *Nf2-iso2*$^{-/-}$ mice. Axonal targeting also appeared to be normal in merlin isoform–specific knockout mice, despite the morphological axonal alterations. Silver impregnation and immunohistochemical staining for acetylcholine receptors and myelinated nerve fibers of gastrocnemius muscles did not show relevant alterations concerning muscular structure or nerve targeting (**Fig. 4e**), indicating proper muscle innervation in *Nf2-iso2*$^{-/-}$ mice.

Given that phosphorylation events equate to addition of repulsive negative charges, neurofilament phosphorylation results in a larger distance between single neurofilament molecules[4]. Accordingly, axons of both heterozygous and homozygous *Nf2-iso2*$^{-/-}$ mice showed decreased interfilament distances as a result of reduced neurofilament phosphorylation (**Fig. 5a,b**). In contrast, *Nf2-iso1*$^{-/-}$ axons showed only a slight reduction in interfilament spacing. Again, comparable effects of merlin-iso2 loss could be detected in young mice at P7 (**Fig. 5c**).

As merlin has important tumor suppressive functions in Schwann cells of the PNS[19], axonal structure and shape alterations in *Nf2-iso2*$^{-/-}$ mice could be indirectly determined by modified Schwann cell signals. In an established NF2 mouse model in which both merlin isoforms are conditionally deleted in Schwann cells (*Mpz-cre; Nf2*$^{loxP/loxP}$ mice)[20], neurofilament phosphorylation was slightly increased, as was the distance between single neurofilaments (**Fig. 5d** and **Supplementary Fig. 8c**). These findings indicate that the described axonal changes in *Nf2-iso2*$^{-/-}$ sciatic nerves are of axonal origin and are not a product of merlin loss in Schwann cells.

We next tested whether the described morphological alterations are causative for neuropathic symptoms *in vivo*. Hot plate testing measuring pain sensitivity revealed that both heterozygous and homozygous *Nf2-iso2*$^{-/-}$ mice had prolonged withdrawal latencies to thermal stimuli compared with wild-type littermates and *Nf2-iso1*$^{-/-}$ mice (**Fig. 6a**), indicating thermal hypoalgesia and impaired responses to noxious thermal stimuli. Rotarod testing revealed that *Nf2-iso2*$^{-/-}$ mice also displayed deficits in motor function. After 5 d of training, they had a mean latency to fall of 115 s compared with 217 s for wild-type littermates (**Fig. 6b**). Even *Nf2-iso2*$^{+/-}$ mice showed a relevant phenotype (155 s).

Electrophysiological measurements on sciatic nerves *in vivo* revealed similar nerve conduction velocities (mainly determined by myelination and reduced in demyelinating neuropathies) in *Nf2-iso1*$^{-/-}$ and *Nf2-iso2*$^{-/-}$ mice (**Fig. 6c**). In contrast, compound muscle action potential amplitudes (reflecting axonal functionality) were greatly reduced in *Nf2-iso2*$^{-/-}$ mice, indicative of axonal neuropathy (**Fig. 6d**). Apart from minor effects following proximal stimulation (possibly because of additional alterations in other tissues as a result of complete isoform-specific knockout of merlin), merlin-iso1 loss had no relevant influence (**Fig. 6d**). These results clearly correlate both homozygous and heterozygous merlin-iso2 inactivation with axonal neuropathy development. These findings are consistent with clinical findings suggesting that polyneuropathy in NF2 patients occurs in the absence of associated tumors (schwannomas)[8,21] and that germline *NF2* mutations cause merlin haploinsufficiency and polyneuropathy in patients[22].

NF2 patient–derived mutations and specimens

We analyzed sural nerve biopsy sections from NF2 patients carrying germline *NF2* mutations who presented clinically with severe neuropathy[21]. Immunohistochemical analysis revealed reduced phospho-neurofilament staining per vital axon compared with healthy control biopsies (**Fig. 7a** and **Supplementary Fig. 9a**). Ultrastructural analysis revealed intrinsic axonal structure abnormalities that closely resembled those of *Nf2-iso2*$^{-/-}$ mice *in vivo* and neurons *in vitro*. Sural nerve axons of the same patients exhibited reduced interfilament distances compared with healthy control samples (**Supplementary Fig. 9b**). In addition, non-myelinated fibers frequently displayed irregularly shaped axons containing accumulations of condensed mitochondria and neurofilaments (**Fig. 7b**), as well as aggregations of pleomorphic vesicles and dense bodies (**Fig. 7c**) that could not be found in biopsies of healthy control individuals (**Fig. 7d**).

In vitro, the C-terminal nonsense *NF2* mutation C784T, which was previously reported to provoke axonal type neuropathy determined by electrophysiological means[8], could not induce neurofilament

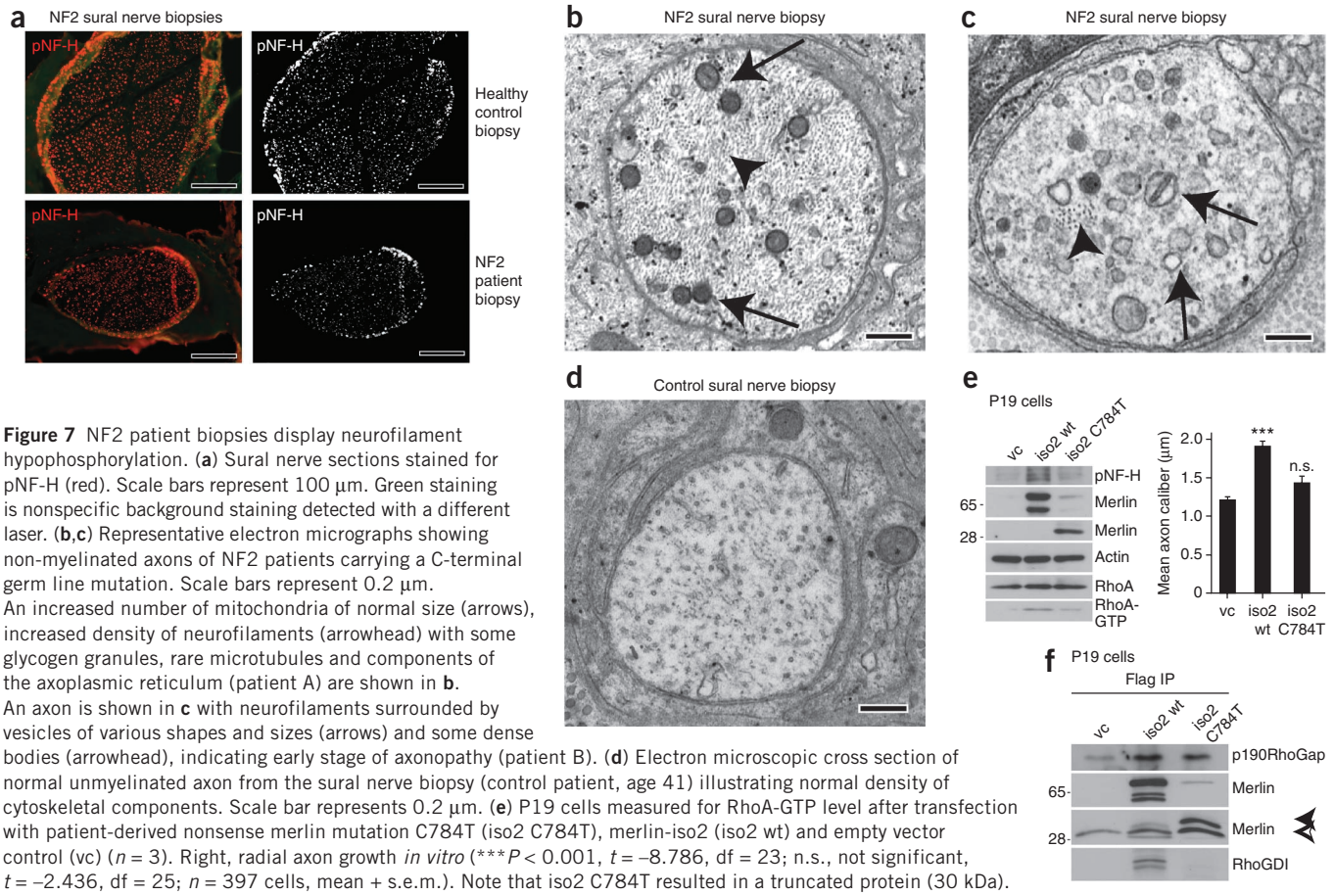

Figure 7 NF2 patient biopsies display neurofilament hypophosphorylation. (**a**) Sural nerve sections stained for pNF-H (red). Scale bars represent 100 µm. Green staining is nonspecific background staining detected with a different laser. (**b**,**c**) Representative electron micrographs showing non-myelinated axons of NF2 patients carrying a C-terminal germ line mutation. Scale bars represent 0.2 µm. An increased number of mitochondria of normal size (arrows), increased density of neurofilaments (arrowhead) with some glycogen granules, rare microtubules and components of the axoplasmic reticulum (patient A) are shown in **b**. An axon is shown in **c** with neurofilaments surrounded by vesicles of various shapes and sizes (arrows) and some dense bodies (arrowhead), indicating early stage of axonopathy (patient B). (**d**) Electron microscopic cross section of normal unmyelinated axon from the sural nerve biopsy (control patient, age 41) illustrating normal density of cytoskeletal components. Scale bar represents 0.2 µm. (**e**) P19 cells measured for RhoA-GTP level after transfection with patient-derived nonsense merlin mutation C784T (iso2 C784T), merlin-iso2 (iso2 wt) and empty vector control (vc) ($n = 3$). Right, radial axon growth *in vitro* (***$P < 0.001$, $t = -8.786$, df = 23; n.s., not significant, $t = -2.436$, df = 25; $n = 397$ cells, mean + s.e.m.). Note that iso2 C784T resulted in a truncated protein (30 kDa). (**f**) P19 cells transfected with Flag-tagged merlin–iso2 (iso2 wt) and C784T mutant (iso2 C784T) ($n = 3$). The white arrowhead indicates an unspecific band in all three lanes. The black arrowhead points to immunoprecipitated truncated merlin (iso2 C784T). For full-length blots and quantitations, see **Supplementary Figure 9**.

phosphorylation or axonal diameter growth in P19 cells (**Fig. 7e**). This mutation was still able to form a complex with p190RhoGAP, but could not bind RhoGDI (**Fig. 7f**), demonstrating the importance of the merlin-RhoGDI complex at least in intact cells. Furthermore, these findings were associated with a loss of RhoA activation (**Fig. 7e**) and indicate that NF2 patients lacking the intact C terminus of one *NF2* allele in neurons fail to regulate Rho-ROCK–dependent neurofilament phosphorylation, leading to insufficient axonal structure maintenance.

DISCUSSION

We found that the ubiquitously expressed tumor suppressor protein merlin (specifically merlin-iso2) functions intrinsically in neurons to regulate axonal integrity and propose that reduced *NF2* gene dosage in axons is relevant in NF2-related polyneuropathy. Specifically, we found that merlin-iso2 regulates RhoA, leading to downstream ROCK activity, which promotes neurofilament phosphorylation and ultimately controls the growth of axonal diameter *in vitro* and axon structure maintenance *in vivo*. Consequently, merlin-iso2 reduction resulted in inhibition of RhoA and neurofilament hypophosphorylation.

Irregular neurofilament phosphorylation has been previously reported to coincide with axonal dysfunction[23] and increased axon vulnerability[24]. Several neuropathic disorders display altered neurofilament phosphorylation levels[2]. Our results highlight importance of neurofilament modulation and provide, to the best of our knowledge, the first *in vivo* evidence that Rho-ROCK signals are important for neurofilament phosphorylation and the consequent maintenance of axonal structure.

While exploring how merlin-iso2 operates in the axon, we identified a merlin-dependent multi-protein complex. Both RhoGDI and p190RhoGAP, important determinants for Rho activity control, were found to associate with neuronal merlin. Our data suggest that axonally expressed merlin-iso2, coupled to neurofilaments, acts as a tethering system, fine-tuning local RhoA signals in the axon. A NF2 patient–derived mutation causing severe polyneuropathy (C784T)[21], which maintains p190RhoGAP interaction, but results in deficient RhoGDI binding, was unable to promote Rho activity and radial axon growth *in vitro*, illustrating the importance of the merlin-RhoGDI complex in intact cells. This scaffold-mediated assembly provides a versatile tool for the spatiotemporal organization of signal transduction. Specific merlin signaling hubs defined to cellular substructures such as axons enable Rho-ROCK signals to promote phosphorylation of neurofilaments, which is important for axon structure.

Our data contribute to the mechanistic understanding of why NF2 patients suffer from polyneuropathy even in the absence of nerve damaging tumors. Merlin was originally identified as a tumor suppressor protein and is known to be involved in gliogenic tumor development. It is assumed, but not proven, that the cause of nerve damaging processes associated with NF2 disease is a result of secondary problems, such as compressive glial cell tumors (schwannomas)[8,22,25] or hyperproliferative Schwann cells (tumorlets)[8]. We found that NF2 patients have axon-intrinsic ultrastructural irregularities and

reduced phosphorylated neurofilaments relative to normal healthy controls, indicating that the nerve damage in NF2 patients develops from an inner axonal process resulting from reduced merlin protein levels. This neuron-intrinsic impairment was verified in our mouse model, in which the specific loss of merlin-iso2, or even a reduction in the merlin-iso2 dosage, resulted in nerve damage and neuropathic symptoms without the appearance of Schwann cell–derived tumors. Despite the described axonal abnormalities, we could not detect classical signs of axon degeneration in *Nf2-iso2*$^{-/-}$ mice. We observed a phenotype resembling 'axonal atrophy', with shrunken and collapsed axons of peripheral nerves as have described previously in the context of neurofilament mutations[18]. We detected neuropathy of axonal origin in mutant mice and propose that the loss of merlin-iso2 leads to a reduction of functional axons.

Our findings are unexpected for this tumor suppressor and relevant for a complete understanding of the spectrum of nervous system abnormalities in the human NF2 disease. It is reasonable to assume that the signaling pathway downstream of merlin that we describe has a broader implication for other hereditary neuropathies whose mechanisms remain elusive. Elucidation of the signaling pathways of radial axonal growth and maintenance is will be necessary to fully understand nerve regeneration and protection from axonal degeneration.

METHODS

Methods and any associated references are available in the online version of the paper.

Note: Supplementary information is available in the online version of the paper.

ACKNOWLEDGMENTS

The authors would like to thank U. Petz, C. Poser and S. Ramrath for their expert technical assistance, H. Rosemann, F. Kaufmann and D. Galendo for their skilled breeding and husbandry of animals, and R.E. Ferner for discussions and support. *Mpz-cre* mice were kindly provided M.L. Feltri (Hunter James Kelly Research Institute). This work was supported by Sonderforschungsbereich 604, Deutsche Forschungsgemeinschaft MO 1421/2–1 and Krebshilfe 107089. A.S. is recipient of a Young Investigator Award from the Children's Tumor Foundation.

AUTHOR CONTRIBUTIONS

A.S. and H.M. conceived and designed the study. H.M. supervised the experimental program and prepared the manuscript. A.S. performed and analyzed the majority of the experiments and prepared the manuscript. S.L.B. performed the nerve section analysis of both knockout mice and patient biopsies, as well as their analysis. M.N.-K. and M.G. generated the *Nf2-iso1*$^{-/-}$ and *Nf2-iso2*$^{-/-}$ mice. R.B. designed the electrophysiological experiments and participated in data acquisition. C.G. and D.H.G. synthesized isoform-specific merlin antibodies. A.Z. and M.J.J. participated in the behavioral analysis of merlin knockout mice and the preparation of primary cell cultures. S.S. conducted nucleotide exchange and binding assays. X.-P.D. and D.B.P. provided tissue samples of *Mpz-cre; Nf2*$^{loxP/loxP}$ mice. C.H. and V.-F.M. provided NF2 patient biopsy sections for immunohistochemistry. C.O.H. provided NF2 patient biopsy sections for ultrastructural analysis. J.W. and J.M.S. performed the ultrastructural analysis of human NF2 patient biopsies.

COMPETING FINANCIAL INTERESTS

The authors declare no competing financial interests.

1. Luo, L. Rho GTPases in neuronal morphogenesis. *Nat. Rev. Neurosci.* **1**, 173–180 (2000).
2. Perrot, R., Berges, R., Bocquet, A. & Eyer, J. Review of the multiple aspects of neurofilament functions, and their possible contribution to neurodegeneration. *Mol. Neurobiol.* **38**, 27–65 (2008).
3. Zhu, Q., Couillard–Despres, S. & Julien, J.P. Delayed maturation of regenerating myelinated axons in mice lacking neurofilaments. *Exp. Neurol.* **148**, 299–316 (1997).
4. de Waegh, S.M., Lee, V.M. & Brady, S.T. Local modulation of neurofilament phosphorylation, axonal caliber and slow axonal transport by myelinating Schwann cells. *Cell* **68**, 451–463 (1992).
5. Dubois, M., Strazielle, C., Julien, J.P. & Lalonde, R. Mice with the deleted neurofilament of low molecular weight (*Nefl*) gene. 2. Effects on motor functions and spatial orientation. *J. Neurosci. Res.* **80**, 751–758 (2005).
6. England, J.D. & Asbury, A.K. Peripheral neuropathy. *Lancet* **363**, 2151–2161 (2004).
7. Asthagiri, A.R. *et al.* Neurofibromatosis type 2. *Lancet* **373**, 1974–1986 (2009).
8. Sperfeld, A.D., Hein, C., Schroder, J.M., Ludolph, A.C. & Hanemann, C.O. Occurrence and characterization of peripheral nerve involvement in neurofibromatosis type 2. *Brain* **125**, 996–1004 (2002).
9. Schulz, A. *et al.* Merlin inhibits neurite outgrowth in the CNS. *J. Neurosci.* **30**, 10177–10186 (2010).
10. Gianola, S. & Rossi, F. Evolution of the Purkinje cell response to injury and regenerative potential during postnatal development of the rat cerebellum. *J. Comp. Neurol.* **430**, 101–117 (2001).
11. Jones–Villeneuve, E.M., McBurney, M.W., Rogers, K.A. & Kalnins, V.I. Retinoic acid induces embryonal carcinoma cells to differentiate into neurons and glial cells. *J. Cell Biol.* **94**, 253–262 (1982).
12. Hashimoto, R. *et al.* Domain- and site-specific phosphorylation of bovine NF-L by Rho-associated kinase. *Biochem. Biophys. Res. Commun.* **245**, 407–411 (1998).
13. Moorman, J.P., Luu, D., Wickham, J., Bobak, D.A. & Hahn, C.S. A balance of signaling by Rho family small GTPases RhoA, Rac1 and Cdc42 coordinates cytoskeletal morphology, but not cell survival. *Oncogene* **18**, 47–57 (1999).
14. Maeda, M., Matsui, T., Imamura, M. & Tsukita, S. Expression level, subcellular distribution and rho-GDI binding affinity of merlin in comparison with Ezrin/Radixin/Moesin proteins. *Oncogene* **18**, 4788–4797 (1999).
15. Yamashita, T. & Tohyama, M. The p75 receptor acts as a displacement factor that releases Rho from Rho-GDI. *Nat. Neurosci.* **6**, 461–467 (2003).
16. Sherman, L. *et al.* Interdomain binding mediates tumor growth suppression by the NF2 gene product. *Oncogene* **15**, 2505–2509 (1997).
17. Bremer, J. *et al.* Axonal prion protein is required for peripheral myelin maintenance. *Nat. Neurosci.* **13**, 310–318 (2010).
18. Elder, G.A., Friedrich, V.L. Jr., Margita, A. & Lazzarini, R.A. Age-related atrophy of motor axons in mice deficient in the mid-sized neurofilament subunit. *J. Cell Biol.* **146**, 181–192 (1999).
19. Giovannini, M. *et al.* Conditional biallelic Nf2 mutation in the mouse promotes manifestations of human neurofibromatosis type 2. *Genes Dev.* **14**, 1617–1630 (2000).
20. Feltri, M.L. *et al.* Conditional disruption of beta 1 integrin in Schwann cells impedes interactions with axons. *J. Cell Biol.* **156**, 199–209 (2002).
21. Hagel, C. *et al.* Polyneuropathy in neurofibromatosis 2: clinical findings, molecular genetics and neuropathological alterations in sural nerve biopsy specimens. *Acta Neuropathol.* **104**, 179–187 (2002).
22. Hanemann, C.O., Diebold, R. & Kaufmann, D. Role of NF2 haploinsufficiency in NF2-associated polyneuropathy. *Brain Pathol.* **17**, 371–376 (2007).
23. Jackson, S.J., Pryce, G., Diemel, L.T., Cuzner, M.L. & Baker, D. Cannabinoid-receptor 1 null mice are susceptible to neurofilament damage and caspase 3 activation. *Neuroscience* **134**, 261–268 (2005).
24. Morrison, J.H. *et al.* A monoclonal antibody to non-phosphorylated neurofilament protein marks the vulnerable cortical neurons in Alzheimer's disease. *Brain Res.* **416**, 331–336 (1987).
25. Iseki, C. *et al. Rinsho Shinkeigaku* [A case of neurofibromatosis type 2 (NF2) presenting with late–onset axonal polyneuropathy] **49**, 419–423 (2009).

ONLINE METHODS

Experimental animals. All mice handled in strict adherence to local governmental and institutional animal care regulations (Thüringer Landesamt für Lebensmittelsicherheit und Verbraucherschutz). *Nf2-iso1*$^{-/-}$ and *Nf2-iso2*$^{-/-}$ mice were generated by M.N.-K. and M.G. (unpublished data) and purchased from Riken BioResource (C57BL/6 background). Average day of birth, on the 19th day of pregnancy, was defined as P0 and adult was defined as P60. Behavior and electrophysiology tests, immunohistochemistry and electron microscopy were carried out on mice or tissue taken from 8-week-old mice unless otherwise stated. All of the mice used for this study were age and gender matched, as well as derived from group housing. Genotyping was performed by PCR of tail biopsies. For *Nf2-iso1*$^{-/-}$ mice, the primers Nf2 insert (5′-CCT CAA GCC CAA GGC AGA AGA-3′) and Nf2 insert2a (5′-CCT CAG AGT GAG GCA GTC TTC TAG G-3′) were used, yielding 267 bp or 391 bp products for wild-type or knockout alleles, respectively. For *Nf2-iso2*$^{-/-}$ mice, primers Nf2 (5′-CAG TAC ACC TGA GGT CAC TGT CTC-3′) and Nf2 insert2a were used to generate 235 bp and 378 bp products for knockout and wild-type alleles, respectively.

Immunohistochemistry. Mice were perfused transcardially using phosphate-buffered saline (PBS), followed by 4% paraformaldehyde (vol/vol) in PBS. Following dissection, brains were post-fixed in the same fixative overnight at 20 °C. Floating sections were cut to 50 µm thicknesses or to 8 µm thickness for paraffin-embedded sections. Floating sections were heated in 10 mM sodium citrate buffer (pH 9) at 80 °C for 30 min and, after cooling, incubated in 2% non-fat dry milk (vol/vol) for 30 min. Sections were treated with 0.5% Triton X-100 (vol/vol) for 30 min and incubated in 0.2% gelatine and 2% goat serum (vol/vol) diluted in PBS for 2 h. Sections were submersed in primary antibody solution overnight at 4 °C. For primary antibodies, we used antibodies to calbindinD-28k (rabbit polyclonal, 1:2,000, Swant, clone CB38), MBP (mouse monoclonal, 1:500, clone MAB384, Millipore Bioscience Research Reagents) phospho-neurofilament (SMI31, 1:500, Hiss Diagnostics), merlin (A-19, 1:200, Santa Cruz Biotechnology), and merlin-iso1 (WA27, 1:100) and merlin-iso2 (WA28, 1:100) (D.H.G.)[26]. The rabbit polyclonal merlin antibodies were raised after repeated immunizations and peptide purification (WA27, C-PQAQGRRPICI; WA28, C-LTLQSAKARVAFFEEL). After vigorous washings, sections were incubated with the secondary antibody solution (Alexa488- and Alexa546-conjugated goat antibodies to mouse or rabbit, 1:500 in PBS, A-11034 and A-11030, Invitrogen) at 20 °C for 2 h. Sections were counterstained using Hoechst 34580 (1 µg ml^{-1} PBS, 5 min), washed for at least 1 h and embedded in Mowiol. Merlin-specific staining was confirmed previously[9] and we tested the antibody to merlin-iso2 antibody on tissues from *Nf2-iso2*$^{-/-}$ mice (**Supplementary Fig. 2**).

Paraffin-embedded sections were rehydrated, boiled in 10 mM sodium citrate buffer (pH 9) for 30 min in a microwave and subsequently treated with 0.5% Triton X-100 for 10 min. Sections were incubated in 0.2% gelatine and 2% goat serum diluted in PBS for at least 2 h. Sections were submersed in the primary antibody solution overnight at 4 °C. For primary antibodies, we used antibodies to phospho-neurofilament (SMI31, 1:500, Hiss Diagnostics), merlin-iso1 (WA-27, 1:100), merlin-iso2 (WA-28, 1:100) and APP (rabbit polyclonal antibody, Calbiochem, 1:500, 171610). After vigorous washings, sections incubated with secondary antibody solution (Alexa488- and Alexa546-conjugated goat antibodies to mouse or rabbit, 1:500 in PBS, Invitrogen) at 20 °C for 2 h. Finally, specimens were washed in PBS, counterstained using Hoechst 34580 (1 µg ml^{-1} PBS, 5 min), dehydrated and embedded.

Immunocytochemistry. P19 cells, primary cerebellar neurons or DRG cells were grown on coverslips and fixed with 4% paraformaldehyde in PBS for 20 min. After washing in PBS, cells were permeabilized with 0.3% Triton X-100 for 1 min and incubated for 2 h in 1% bovine serum albumin (vol/vol). Cells incubated with primary antibodies at 20 °C for 1 h. For primary antibodies, we used antibody to phosphor-neurofilament (SMI31, 1:200, Hiss Diagnostics), RhoGDI (A-20, 1:100, Santa Cruz Biotechnology), growth-associated protein (GAP-43, clone H-100, 1:400, Santa Cruz Biotechnology), APP (rabbit polyclonal antibody, Calbiochem, 1:100), merlin-iso1 (WA-27, 1:50), merlin–iso2 (WA-28, 1:50) and p190RhoGAP (mouse monoclonal antibody, Sigma, clone D2D6, 1:100). After extensive rinsing in PBS, cells were incubated with secondary antibodies (Alexa488-conjugated antibody to rabbit, 1:500; Alexa546-conjugated antibody to mouse, 1:500) for 1 h. Cells were washed in PBS and counterstained with Hoechst 34580 (1:1,000 in PBS) for 5 min. Cells were mounted on cover plates with a Mowiol-based mounting medium.

Developmental appearance of merlin in Purkinje cell axons. Axonal expression of merlin-iso2 determined by colocalization of merlin (iso2) with the Purkinje cell–specific marker calbindin. Continuous calbindin-positive signals in the granular layer of the mouse cerebellum with lengths of more than 20 µm were analyzed for additional merlin staining. Note the methodical difference with apparent discrepant results in a previous study[9]. There, the appearance of merlin in the proximal axon initial segment was monitored.

Immunoblotting. Immunoblotting was performed as described previously[27]. For primary antibodies, we used antibodies to merlin (clone A-19, 1:500), actin (clone I-19, 1:1,500, Santa Cruz Biotechnology), RhoA (1:500, Upstate), phospho-neurofilament (SMI31, 1:500, Hiss Diagnostics), pan-axonal neurofilament (SMI312, 1:500, Hiss Diagnostics), Flag (clone M2, 1:1,000, Sigma-Aldrich), RhoGDI (A-20, 1:500, Santa Cruz Biotechnology), merlin-iso1 (WA-27, 1:500), merlin-iso2 (WA-28, 1:500) and p190RhoGap (mouse monoclonal antibody, Sigma, clone D2D6, 1:1,000). Western blot results were quantified using gel analysis software by ImageJ. Density values were normalized to actin and appropriate controls of transfection or wild-type tissue.

Pulldowns to detect active RhoA. A detection kit was used (Active Rho Pull-Down and Detection Kit, Pierce Biotechnology) according to manufacturer instructions. Precipitates and total lysates were resolved on a 10% SDS-PAGE gel and immunoblotted using antibody to RhoA (1:500, Upstate). Total lysates were used as loading controls. Pulldown assays were repeated at least three times in each case.

P19 cell culture. P19 cells[11] purchased from ATCC (CRL-1825) maintained in Dulbecco's modified Eagle's medium supplemented with 10% fetal calf serum (vol/vol). Induction of neuronal phenotype, aggregates were generated on bacterial-grade dishes and treated with 5×10^{-7} M all-trans retinoic acid (Sigma) for 4 d. Cells were re-plated on cell culture dishes in the absence of retinoic acid.

Primary dissociated cerebellar cultures. Primary dissociated cerebellar cultures (referred to as cerebellar granular cells) were established from cerebellar tissue of 8-d-old pups (C57BL/6 mice) as described previously[28]. Cells were grown at a density of 200,000 cells cm^{-2} in defined neurobasal medium with B27 supplement (Invitrogen).

DRG culture. Cells were prepared from 4–6-d-old mice (P4–6) as described[29]. Arabinofuranosyl cytidine (Sigma, C1768, working concentration of 10 µM) was used to assure glial-free conditions.

Transfection procedures. P19 cells were transfected 3–4 d after plating using Lipofectamine 2000 (Invitrogen) according to the manufacturer's protocol. Transfection efficiency averaged around 45 to 50%. For siRNA knockdown experiments, primary cells were transfected using Dharmafect 3 according to the manufacturer's instructions (Dharmacon, Thermo Scientific). Using siGLO RNA, a transfection rate of 75% was obtained. For overexpression studies, primary neurons were transfected according to a method described previously[30].

For inhibition of merlin expression, the following oligonucleotides were used: si-nf2 5′-UAC CGA GCU UCG ACA UUA UUG-3′ (knockdown of both major merlin isoforms), si-iso1 5′-AAA GAA GGC CAC UCG GGA CUU-3′, si-iso2 5′-UAG GUC UUC UGC CUU GGG CUU-3′ and scr-nf2 5′-AAU CCG GUU GCA UAG UUC AUG-3′ (untargeted control). For RhoGDI knockdown, siRNA was purchased from Santa Cruz Biotechnology (sc-36416). For overexpression of merlin, pcDNA3-based *Nf2* full-length sequences for isoform 1 and 2 was used. Backbone vector pcDNA3 used as control. Merlin fragment constructs used: N-terminus amino acids (aa) 1–299; C-terminus merlin-iso1 aa 300–595; C-terminus of merlin-iso2 aa 300–590. QuikChange Site–Directed Mutagenesis Kit (Stratagene) was used according to the manufacturer's instructions.

For knockdown of p190RhoGAP, we used the pGIPZ plasmid containing shRNA against the *ARHGAP35* gene according to manufacturers recommendation (Open Biosystems, Oligo ID: V3LHS_349456, GeneID: 2909; antisense

doi:10.1038/nn.3348

sequence: TCCAGGTAGACATAGTCCT). The shRNA was directed against the human gene, but is homologous to rat and mouse. In brief, shRNA was co-transfected with pMD.G-VSVG and pCMVdelR8.91 packaging plasmids into HEK293T cells using Lipofectamine 2000. After 48 h, the supernatant containing viral particles was harvested, sterile filtered and used for transduction of DRG cells. Thus, DRG cells were incubated with viral particles in DMEM/5% fetal bovine serum for 16 h and subsequently grown in DMEM/10% fetal bovine serum.

Quantification of axonal diameter *in vitro*. Diameters of axonal processes of differentiated P19 cells, primary cerebellar neurons and DRG cells were measured 3 d after transfection. To identify axonal processes, cells were co-stained with the axonal markers GAP-43 and phospho-neurofilaments p(NF-H) (**Supplementary Fig. 3a**). Using the ImageJ plugin NeuronJ, axons longer than a cell soma were measured and scaled in micrometers. Processes that could be clearly distinguished from processes of neighboring cells were evaluated. Changes of axon calibers *in vitro* are also referred to as changes in radial axon growth.

Microscopy and image acquisition. Confocal images were obtained with a Leica TCS SP5 laser-scanning microscope. Images were acquired with a 40× objective (HCX APO 40.0X 0.75 DRY, NA = 0.75) at a pinhole size of three airy discs and a resolution of 0.73 × 0.73 × 0.50 μm^3. Images were taken from a single optical planes (voxel size = 189 nm). Epifluorescent images of dissociated neurons were obtained with a Leica DMIRE2 microscope equipped with a Leica DFC350FX camera. All digital processing was performed using Adobe Photoshop 6.0. For all images, only linear adjustments of the brightness and contrast were performed.

RhoA activation. Rho activator #CN01 (Cytoskeleton) was used according to the manufacturer's recommendations.

Analysis of axonal caliber and myelination in merlin knockout mice. Analysis was carried out on semi-thin and thin sections of the sciatic nerve obtained from transcardially perfused *Nf2-iso1*$^{-/-}$, *Nf2-iso2*$^{-/-}$, *Nf2-iso1*$^{+/-}$, *Nf2-iso2*$^{+/-}$ and wild-type mice. Mice were perfused with a solution containing 3% paraformaldehyde and 3% glutaraldehyde (vol/vol) in 0.1 M phosphate buffer (pH 7.4). Sections were post-fixed for 1 h and kept in fixative that included 3% sucrose (vol/vol). Sections were obtained from the mid part of the sciatic nerve reaching from gluteal to the popliteal regions. Sectioning and staining was performed as described[31]. Images of toluidine blue were stained semithin sections taken using an Axioskop 2 MOT (Carl Zeiss) equipped with a 100× immersion oil objective and an Olympus XC50 digital camera (Olympus). Standardized settings for camera sensitivity, resolution (2,576 × 1,932 pixels) and brightness of illumination were used for all micrographs. Thin sections were analyzed with an electron microscope (EM910, Carl Zeiss) equipped with an integrated TRS 1K digital camera (Carl Zeiss). Image analysis was carried out using ImageJ version 1.43u. RGB color images obtained from semi-thin sections were split into single channels, and the green channel was chosen for measurements. The picture was contrasted using the auto function. Using the freehand selection tool, the axon and the myelin was grossly circumscribed and the area was adapted using the ABSnake PlugIn (gradient threshold varied between 20 and 30, 10–20 iterations per image). Low-contrasted myelin sheaths were surrounded manually. Based on measured areas, we calculated the thicknesses of the axons and myelin sheaths. Providing a measure for bending of the transversely cut axonal surface, the axon was surrounded as described above and solidity factor was measured using the implemented ImageJ software tools (shape descriptor). Solidity factor describes the area covered by a given structure in relation to the smallest convex area, which covers this structure, that is, the solidity factor of a round circle or ellipse would be 1, while whereas circle with an invagination would give a factor smaller than 1. This solidity factor is superior to the circularity factor often used for measuring changes in surface structures, as it provides a factor to measure changes in surface curvatures independent of the plane of section. Changes of axon structure *in vivo* are also referred to as axon structure maintenance or integrity. Three pairs of mice from the same litter were used for experiments. Electron microscopical images were taken from 50-nm-thick sections. Neurofilaments are easily identified by size and compact structure. The positions of all neurofilaments in a defined area covering only tangentially cut neurofilaments were measured and distances to their neighbors evaluated. The nearest neighbor of a neurofilament was defined as the average distance of the three nearest neighbors of a neurofilament. The values provided in **Figure 5b–d** are derived from 300 to 800 distances measured per genotype. At least two mice were taken per genotype. Axon calibers were classified as described previously[32].

Muscle preparations and immunostainings. Preparations were carried out as described before[33]. BTX (Invitrogen, conjugated to Texas Red) was used at a concentration of 1 $\mu g\ ml^{-1}$, and antibody to N52 (Sigma) was used at a dilution of 1:500. Silver staining was done as described[34]. Images were taken with standard bright-field upright microscopes. Images of fluorescent stains were taken using the Leica laser-scanning microscope LSM TCS SP2. Pictures shown are maximum projections of ten images taken at a distance of 1 µm.

Co-immunoprecipitation. Co-immunoprecipitation studies were performed as described previously[27].

Kinase screening assay. We selected 23 serine/threonine kinases on the basis of reports of their association with merlin and/or neurofilament signaling (**Supplementary Table 1**). Appropriate siGENOME SMARTpool duplexes (Thermo Fisher) targeting kinases were transfected into neuronally differentiated P19 cells. Medium was replaced after 24 h, following plasmid transfection of either an empty vector control or merlin-iso2. After 2 additional days, cells were lysed, and subjected to SDS-PAGE and immunoblotting to determine the phosphorylation state of heavy subunit neurofilaments (pNF-H). Consistent results were obtained in three consecutive experiments in 24-well plate format.

Sural nerve biopsies of NF2 patients. Biopsy sections for immunohistochemistry were provided by C.H. For phospho-neurofilament analysis, specimens of two healthy control males (57 and 52 years of age) were compared with nerve tissue from two NF2 patients (both 36 years of age), referred to as patients 718 and 21.3 in ref. 21. Sections were stained for phosphorylated neurofilament epitopes using antibody to SMI31 (**Fig. 7a**). Monochrome single-channel images were excused from fluorescent background staining by threshold setting to a range of 95 to 255 (**Fig. 7a**). By means of ImageJ plugin Analyze Particles, total area covered by phospho-neurofilament staining was determined as $pixel^2$ per μm^2 and subsequently divided by the number of vital axons. Taking the total axon number into account, the decrease was not simply a result of loss of fibers. Quantifications of interfilament distances (**Supplementary Fig. 9b**) was performed as described above.

NF2 sural nerve biopsies for ultrastructural analysis of non-myelinated fibers (mutation in patient A: A1447-2G, age 37; mutation in patient B: 1594 ins3 del59, age 27) were kindly provided by C.O.H. Nerve specimens were fixed in 3.9% phosphate-buffered glutaraldehyde, embedded in epoxy resin and processed for electron microscopy as described previously[23].

The immunohistochemical and ultrastructural studies were performed on archival tissue that was processed and diagnosed in the Institutes of Neuropathology in Hamburg and Aachen. According to the law for hospitals in Hamburg (Germany) and North Rhine–Westphalia (Germany), samples of closed cases that were processed and investigated in a medical institution may be used for research purposes by the same institution without need for a separate written informed consent from the patients.

GST-pulldown assays. GST-RhoGDI (in pGEX2T vector backbone). For pulldown assays from bacteria lysates, frozen pellets of bacteria induced for protein expression were resuspended and lysed in buffer containing 50 mM Tris pH 7.5, 100 mM NaCl, 0.5% CHAPS (vol/vol) and protease inhibitor cocktail. Samples were sonicated on ice for 5–10 min and cell debris was collected for 15 min at 12,000*g* and 4 °C. Cleared lysates were diluted in 1 ml of pulldown buffer and incubated with GST alone or GST-tagged proteins bound to glutathione beads for 1.5-2 h rotating at 4 °C. Four washing steps were performed with 1 ml of pulldown buffer. Simultaneously, beads were spun down at 5,000*g* for 30 s and boiled in 2× SDS sample buffer and analyzed by subsequent SDS-PAGE and western blotting.

Protein interactions *in vitro*. We applied 1.5 µg of purified His-RhoGDIα (aa 24–204, Fitzgerald) or 3 µg bovine serum albumin (BSA) point-wise on dry nitrocellulose membrane. Membrane was blocked in 5% skimmed-milk (vol/vol)

in TBS-Tween for 1 h followed by 2.5-h incubation with 5 μg ml^{-1} purified Merlin FERM domain or BSA in 0.5% CHAPS, 50 mM Tris (pH 7.5) and 100 mM NaCl at 20 °C, respectively. After three washes with TBS-Tween, membranes were treated with antibody to merlin (A-19, 1:750) for 1 h at 20 °C, followed by incubation with horseradish peroxidase–coupled antibody to rabbit (1:2,000) for 1 h.

Nucleotide exchange assay. Assay was performed on the basis of a Rho GEF exchange assay kit (Cytoskeleton BK100) according to manufacturers recommendation. In brief, 2× exchange reaction buffer contained 1.5 μM mant-GTP in 40 mM Tris (pH 7.5), 100 mM NaCl and 20 mM $MgCl_2$. Samples containing a final concentration of 2 μM RhoA, 3 μM His-RhoGDI (aa 24–204, Fitzgerald) and 4 μM merlin FERM domain (aa 1–313, 50 mM Tris (pH 7.5), 300 mM NaCl) were pre-incubated on ice for 30 min in a black 384 round bottom well plate (Corning). The 2× exchange buffer was added to a final concentration of 0.75 μM of mant-GTP. Samples immediately analyzed with a Mithras LB 940 Multimode Microplate Reader (Berthold Technologies) at 20 °C. Fluorescence emission was recorded at 460 nm after excitation with lamp energy of 5,000 (5.72 W) at 355 nm every 20 s. The hDbs GEF (human Dbl Big Sister) fragment was added to a final concentration of 0.5 μM and a total reaction volume of 15 μl. Measurement measured for 6 h. Control protein samples components replaced by BSA.

Rotarod test. Measures motor coordination and proprioception. Determines time that mice can stay on a rotating rod, referred to as latency to fall. To increase test sensitivity, we used a program accelerating the rod from 1 to 50 rpm in 4.2 min (accelerates at 1 rpm per 5 s). Each mouse underwent the same 5-d procedure passing two sessions per d including two trials each session. Mice still on the apparatus at 252 s were scored as 252 s. Rotating on the rod for two consecutive rotations without running equaled falling event. Day 5 performances were used for statistical analysis using Bonferroni correction.

Hot plate test. The hot plate test measures response to thermal stimuli. Mice were placed on a horizontal surface that was heated to 55 °C. Subsequently, the latency for hind paw withdrawal was measured, with a 60-s cut-off time to prevent severe tissue damage.

Electrophysiology. An investigation of the sciatic nerve conduction characteristics in 8-week-old mice was performed as described previously[35] in a blinded way. Statistical analysis, results of six gender-matched mice per genotype were quantified.

Statistical evaluation. Differences between *Nf2-iso1*$^{-/-}$ and *Nf2-iso2*$^{-/-}$ mice and their appropriate wild-type littermates were determined. For all quantitative analyses, we compared two independent groups of experiments. To demonstrate their comparable distribution, we performed Levene's test for equal variances. Comparisons between groups were made with unpaired *t* tests unless stated otherwise (SPSS software, Statistical Package for the Social Sciences). For each experiment we calculated the *P* value, the *t* value and the degrees of freedom. Differences were considered to be significant when $P < 0.05$. All values are presented as means and their s.e.

26. Scherer, S.S. & Gutmann, D.H. Expression of the neurofibromatosis 2 tumor suppressor gene product, merlin, in Schwann cells. *J. Neurosci. Res.* **46**, 595–605 (1996).
27. Morrison, H. *et al.* The NF2 tumor suppressor gene product, merlin, mediates contact inhibition of growth through interactions with CD44. *Genes Dev.* **15**, 968–980 (2001).
28. Baader, S.L. & Schilling, K. Glutamate receptors mediate dynamic regulation of nitric oxide synthase expression in cerebellar granule cells. *J. Neurosci.* **16**, 1440–1449 (1996).
29. Malin, S.A., Davis, B.M. & Molliver, D.C. Production of dissociated sensory neuron cultures and considerations for their use in studying neuronal function and plasticity. *Nat. Protoc.* **2**, 152–160 (2007).
30. Watanabe, S.Y. *et al.* Calcium phosphate–mediated transfection of primary cultured brain neurons using GFP expression as a marker: application for single neuron electrophysiology. *Neurosci. Res.* **33**, 71–78 (1999).
31. Jankowski, J., Miething, A., Schilling, K. & Baader, S.L. Physiological purkinje cell death is spatiotemporally organized in the developing mouse cerebellum. *Cerebellum* **8**, 277–290 (2009).
32. Michailov, G.V. *et al.* Axonal neuregulin-1 regulates myelin sheath thickness. *Science* **304**, 700–703 (2004).
33. Mundegar, R.R., Franke, E., Schafer, R., Zweyer, M. & Wernig, A. Reduction of high background staining by heating unfixed mouse skeletal muscle tissue sections allows for detection of thermostable antigens with murine monoclonal antibodies. *J. Histochem. Cytochem.* **56**, 969–975 (2008).
34. Mulisch, M.W.U. *Romeis–Mikroskopische Technik* (Spektrum Akademischer Verlag, 2010).
35. Xia, R.H., Yosef, N. & Ubogu, E.E. Dorsal caudal tail and sciatic motor nerve conduction studies in adult mice: technical aspects and normative data. *Muscle Nerve* **41**, 850–856 (2010).

doi:10.1038/nn.3348